Identification of noncalcified coronary plaque characteristics using machine learning radiomic analysis of non-contrast high-resolution computed tomography

Mariusz Kruk[1], Łukasz Wardziak[1], Marton Kolossvary[2, 3], Pal Maurovich-Horvat[4], Marcin Demkow[1], Cezary Kępka[1]

[1]Coronary and Structural Heart Disease Department, National Institute of Cardiology, Warszawa, Poland
[2]Gottsegen National Cardiovascular Center, Budapest, Hungary
[3]Physiological Controls Research Center, University Research and Innovation Center, Óbuda University, Budapest, Hungary
[4]MTA-SE Cardiovascular Imaging Research Group, Heart and Vascular Center, Semmelweis University, Budapest, Hungary

Correspondence to:
Mariusz Kruk, MD, PhD, Coronary and Structural Heart Disease Department, National Institute of Cardiology, Alpejska 42, 04–628 Warszawa, Poland,
phone: +48 22 34 34 342,
e-mail: mkruk@ikard.pl

DOI: 10.33963/v.kp.97206

Received:
December 15, 2022

Accepted:
August 28, 2023

Early publication date:
September 3, 2023

ABSTRACT

Background: Novel imaging and analysis techniques may offer the ability to detect noncalcified or high-risk coronary plaques on a non-contrast computer tomography (CT) scan, advancing cardiovascular diagnostics.

Aims: We aimed to explore whether machine learning (ML) radiomic analysis of low-dose high-resolution non-contrast electrocardiographically (ECG) gated cardiac CT scan allows for the identification of noncalcified coronary plaque characteristics.

Methods: We prospectively enrolled 125 patients with noncalcified plaques and adverse plaque characteristics (APC) and 25 controls without visible atherosclerosis on coronary CT angiography (CCTA). All patients underwent non-contrast CT exam before CCTA. Four hundred and nineteen radiomic features were calculated to identify the presence of any coronary artery disease (CAD), obstructive CAD (stenosis >50%), plaque with ≥2 APC, degree of calcification, and specific APCs. ML models were trained on a training set (917 segmentations) and tested (validation) on a separate set (292 segmentations).

Results: Among the radiomic features, 88.3% were associated with a plaque, 0.9% with obstructive CAD, and 76.4% with the presence of at least two APCs. Overall, 80.2%, 88.5%, and 36.5%, of features were associated with calcified, partially calcified, and noncalcified plaques, respectively. Regarding APCs, 61.1%, 61.8%, 84.2%, and 61.3% of features were associated with low attenuation (LAP), napkin-ring sign (NRS), spotty calcification (SC), and positive remodeling (PR), respectively. ML models outperformed conventional methods for the presence of plaque obstructive stenosis, and the presence of 2 APCs, as well as for noncalcified plaques and partially calcified plaques, but not for calcified plaques. ML models also significantly outperformed identification of LAP and PR, but neither NRS nor SC.

Conclusion: Radiomic analysis of non-contrast cardiac CT exams may allow for the identification of specific noncalcified coronary plaque characteristics displaying the potential for future clinical applications.

Key words: adverse plaque characteristics, atherosclerosis, coronary CTA, radiomics

INTRODUCTION

According to recent cardiology guidelines, coronary computed tomography angiography (CCTA) plays a leading role in diagnostics of symptomatic patients with chest pain [1]. Traditional CCTA image analysis is based on radiodensity, qualitative and quantitative stenosis, and plaque assessment and provides high negative predictive value to exclude significant stenosis or coronary artery disease (CAD) [2]. CCTA also allows for the identification of adverse plaque characteristics

WHAT'S NEW?

Diagnosis of coronary atherosclerosis on computed tomography angiography (CT) has significant therapeutic implications. Novel imaging and analysis techniques may offer the ability to detect disease signs with less risk for the patient. We explored whether artificial intelligence may help to detect noncalcified or high-risk coronary plaques on non-contrast CT scan. The use of machine learning radiomic models allowed for improved detection of coronary plaques, obstructive stenosis, or noncalcified plaques, compared to conventional methods, based on non-contrast cardiac CT scan. Also, machine learning radiomic models improved identification of adverse plaque characteristics, including low attenuation plaque or positive remodeling. To sum up, artificial intelligence improves detection of noncalcified high-risk coronary plaques on non-contrast CT scan, advancing cardiovascular diagnostics.

(APCs) predictive of outcomes, including napkin ring sign, presence of low attenuation plaque, positive remodeling, or spotty calcifications [3]. Technological progress in CT imaging encompasses both post-processing methods and hardware technologies. CT-based images contain much more information than can be accessed by the human eye and traditional analytic tools. Radiomics explores spatial distribution of signal intensities and pixel interrelationships and decodes latent patterns facilitating precision phenotyping of diseases based on imaging [4]. Regarding the hardware, the most advanced contemporary CT scanners enable acquiring high-resolution, electrocardiographically (ECG) gated coronary scans with low radiation doses.

We performed a proof-of-concept study, exploring whether machine learning (ML) radiomic analysis of low-dose high-resolution non-contrast ECG-gated coronary artery CT scan allows for the identification of specific coronary pathologies, including noncalcified plaque, degree of calcification of the plaque, obstructive stenosis, and APCs. The ability to use non-contrast CTs to characterize CAD could potentially translate into future clinical applications, like improved risk assessment or pre-screening of individuals before CCTA exams, leading to a paradigm change in coronary diagnostics with CT.

METHODS

Study design and participants

This was a prospective single-center pilot study. The institutional review board approved the study protocol, and all study participants provided written informed consent. All procedures used in this study were in accordance with local regulations and the Declaration of Helsinki.

The study aimed to enroll 125 study patients with coronary atherosclerosis and with the presence of at least one noncalcified coronary plaque exhibiting APC (inclusion criterion) and 25 controls without visible atherosclerosis on CCTA. Hypertension was defined as a systolic blood pressure ≥140 mm Hg, diastolic blood pressure ≥90 mm Hg or use of blood-pressure-lowering medication. Current smokers were defined as individuals who had smoked any tobacco in the previous 12 months. Hypercholesterolemia was defined as a fasting cholesterol level ≥5.2 mmol/l or statin/fibrate treatment before the index examination. Diabetes was defined as a reported diagnosis from the treating physician, use of insulin, oral hypoglycemic or insulin-sensitizing agent, or fasting glucose level ≥7 mmol/l. Family history of coronary artery disease was defined as the occurrence of myocardial infarction, coronary revascularization, stroke, or sudden death before the age of 55 years in male or 65 years in female 1st-degree relatives.

Between June 2018 and December 2020, we selected 174 patients from 8250 patients undergoing CCTA examination at our center based on the above criteria; 24 refused to participate. The 150 remaining were enrolled within 30 days of CCTA.

There were no prior studies on radiomic analysis of non-contrast coronary CT scans, not permitting appropriate power calculations for sample size. A patient sample including 125 subjects with at least one noncalcified plaque with APC plus 25 subjects without coronary atherosclerosis (with the assumption that at least 3 plaques per patient are available for analysis) was carefully considered based on previous radiomic analyses, our study aims, and also factoring in feasibility of segmentation work [5–7].

Coronary CT protocol

CCTA scans were performed with a 3rd generation 2 × 192 slice (SOMATOM® Force, Siemens Healthineers AG) dual-source CT scanner. Sublingual nitrates (0.8 mg) were administered routinely to all patients before any scan. In patients with heart rate <70 before the scan and fulfilling the clinical screening criteria, non-contrast high-resolution CT examination was performed before the CCTA study: prospectively ECG-triggered high-pitch spiral (Turbo Flash) acquisition was performed in a craniocaudal direction at 90 kV using and 300 mAs. Images were reconstructed using iterative reconstruction strength ADMIRE 3 (ADMIRE, Siemens Healthcare) with 0.6 mm slice thickness, and an increment of 0.6 mm medium soft convolution kernel (Bv36). Next, standard CCTA examination was performed. The CT examinations were then reviewed using commercially available software (Syngo Via, Siemens Healthcare) for fulfilling CT entry/exclusion criteria by two cardiologists (MK/CK) experienced in CCTA evaluation.

CAD assessment and segmentation

A coronary plaque was defined as any discernible coronary artery wall thickening identifiable in at least two perpendicular imaging planes, causing at least 10% luminal stenosis in a vessel with reference diameter ≥2.5 mm [8, 9], and the applied high-risk criteria included the presence of napkin ring sign (a plaque cross-section with a central area of low CT attenuation, which is surrounded by ring-shaped higher attenuation plaque tissue), or low attenuation plaque (a plaque cross-section with a visible area of low CT attenuation, with confirmed presence of voxels <30 Hounsfield units [HU]) and positive remodeling (an outer vessel diameter >10% than the mean of the diameter of the segments immediately proximal and distal to the plaque), and spotty calcification (a <3 mm calcified plaque component) [10]. In 125 enrolled patients, all coronary plaques and normal (without visible atherosclerosis) coronary artery segments were investigated. In control patients, two proximal coronary segments with the fewest motion artifacts were selected for analysis. The analyzed segments were carefully paired on contrast and non-contrast studies using anatomic landmarks (side branches, calcifications). CT image processing was performed at the core lab using plaque segmentation software (QAngioCT, version 3.2; Medis Medical Imaging Systems bv), as reported previously [11]. The segmentation mask encompassed the whole vessel (lumen plus wall), and it was extracted in the original image space for radiomic analysis as DICOM (Digital Imaging and Communications in Medicine) images.

CCTA-based outcomes

The following plaque-based outcomes were chosen for modeling purposes:

1. General categories based on the presence of any plaque, obstructive CAD (>50% luminal stenosis), or plaque with ≥ 2 adverse plaque characteristics (APCs).
2. Categories based on plaque composition, including calcified, partially calcified, or noncalcified plaque.
3. Categories based on the presence of specific APCs, including low attenuation plaque, positive remodeling, napkin-ring sign, or spotty calcification [11].

Radiomic calculations

Following segmentation, the resulting 3D volumes of interest (VOI) were loaded into open source Radiomics Image Analysis (RIA, v.1.6.0) software [12]. Altogether, 44 first-order parameters describing the histogram of HU values of the VOI were calculated. We also discretized our HU values using 8, 16, and 32 equally sized bins to calculate texture-based metrics. For each discretized image, 114 gray level co-occurrence matrix and 11 gray level run length matrix derived parameters were calculated to enumerate texture. Altogether, 419 radiomic features were calculated to describe the morphology of each lesion.

ML validation

To validate our findings using conventional statistical techniques, we tested whether ML models using the radiomic features as inputs could identify the plaque characteristics in a test set. For this, we randomly divided our patients into a training set (75%: 110 of 147 individuals) with 917 segmentations and a separate test set (25%: 37 of 147 individuals) with 292 segmentations. The test set was only used at the end to evaluate the performance of the ML models following training.

Overall, seven ML models were trained using a previously described ML pipeline [13]. The hyperparameters of the regularized logistic regression (L1, L2 penalty), k-nearest neighbors, random forest, naïve Bayes, Gaussian process, decision tree, and fully connected neural network models were randomly chosen from predefined parameter spaces to find the optimal model during the training process. Exact hyperparameter distributions of the models can be found in the published source code [13]. This was repeated 1000 times. The diagnostic accuracy using a given hyperparameter set was defined as the area under the receiver operating characteristic curve (AUC and ROC) evaluated using 5-fold cross-validation. The ML model providing the best results on the training set was then evaluated on the test set. All ML models were built using scikit-learn (v.1.0.1) in the Python environment (v.3.9.7) [14, 15].

Statistical analysis

Continuous variables were presented as means and standard deviations (SD) or medians and interquartile ranges (IQR) as appropriate, while categorical values as frequencies and percentages.

We used linear mixed models (LMM) to account for the intra-patient clustering by adding a random intercept at the patient level to the model using the lm4 package (v 1.1–27). First, we used a univariate LMM to assess whether any of our plaque characteristics are associated with the given radiomic features. Next, as several different factors may influence radiomic signatures, we corrected our LMMs for kVp and mAs settings of the image that might affect radiomic feature values [16]. Furthermore, we corrected for noncalcified (between –100 and 350 HU), low-attenuation noncalcified (between –100 and 30 HU), calcified (above 350 HU), and the total volume of the VOI, as volume is inherently correlated with radiomic features [17].

To model the radiomic signature network describing the latent morphological features of the VOI, we calculated intra-pair similarities between the features. To correct for the clustering, we used Nakagawa's conditional R^2 values from individual LMMs between each feature using the performance package (v. 0.7.2) [18]. We then converted the resulting similarity matrix to a distance matrix defined as $1\text{-}R^2$. This distance matrix was used for hierarchical clustering of the features. We used the gap statistic to derive the optimal number of latent characteristics

(clusters) among our radiomic signatures using the facto-extra package (v 1.0.7).

The ROC of the best ML model for each plaque outcome was compared to the ROC of the volume of the VOI, noncalcified, calcified, and low attenuation noncalcified volumes using the Venkatraman test with the pROC package (v. 1.17.0.1) [19].

A two-sided *P*-value of 0.05 was used for conventional analyses while for all radiomic comparisons, a Bonferroni corrected *P*-value smaller than 0.00012 (0.05/419) was considered significant. All calculations were done in the R environment (v. 4.0.2) [20].

RESULTS

Baseline characteristics

Of 150 enrolled patients, 3 were excluded from analysis due to coronary calcification blooming artifact interfering with the target noncalcified plaque with APC. Therefore, the study group included 147 subjects (85 males, aged 61.6 [10.8] years), in whom 1216 segments were evaluated. In these segments, CAD was present in 671 (55.2%), obstructive CAD in 145 (11.9%), and plaques with at least two adverse characteristics in 217 (17.9%) cases. There were 220 (18.1%) partially calcified plaques and 122 (10.0%) calcified plaques. Considering adverse plaque characteristics, there were 94 (7.7%) plaques with napkin-ring sign, 151 (12.4%) plaques containing spotty calcification, 268 (22.0%) presenting with positive remodeling, and 212 (17.4%) had a low attenuation component.

All patients were white Caucasian, and their baseline characteristics are presented in Table 1.

Table 1. Baseline patient characteristics

	Study group (n = 147)
Clinical characteristics	
Age, years (SD)	61.6 (10.8)
White, n (%)	147 (100)
Weight, kg (SD)	81.0 (16.3)
Height, cm (SD)	167.4 (14.3)
Diabetes, n (%)	15 (10.2)
Hypertension, n (%)	69 (46.9)
Current smoking, n (%)	20 (13.6)
Family history of coronary artery disease, n (%)	12 (8.2)
Hyperlipidemia, n (%)	73 (49.7)
Blood	
Serum creatinine, mg/dl (SD)	0.88 (0.18)
Glucose, mmol/l (IQR)	1.9 (1.7–2.2)
HDL cholesterol, mg/dl (IQR)	1.3 (1.1–1.6)
LDL cholesterol, mg/dl (IQR)	2.6 (2.0–3.2)
Triglycerides, mg/dl (IQR)	1.2 (0.9–1.8)
High sensitivity-CRP, g/l (IQR)	0.13 (0.08–0.29)
Hemoglobin, g/dl (SD)	14.2 (1.2)
Medications	
Antiplatelet agents, n (%)	63 (42.9)
Beta-blocking agents, n (%)	49 (33.3)
Agents acting on the renin-angiotensin system, n (%)	25 (17.0)
Calcium channel blockers, n (%)	13 (8.8)
Statins, n (%)	61 (41.5)
Diuretics, n (%)	12 (8.2)
Anti-diabetic agents, n (%)	15 (10.2)
CT scan	
kV (SD)	84.1 (5.8)
mA (SD)	553.9 (17.0)
CCTA dose, mGy*cm (SD)	520.4 (219.6)
Non-contrast high-resolution CT scan, mGy*cm (SD)	37.0 (4.2)

Abbreviations: CT, computed tomography; CCTA, coronary computed tomography angiography; cm, centimeter; IQR, interquartile range; kV, kilo Volt; mA, mili Amper; mGy, mili Grey, SD, standard deviation

Association between plaque characteristics and radiomic features — univariate analysis

In univariate analysis, we found 90.0% (377/419), 55.8% (234/419), and 80.9% (339/419) of the features to be associated with the presence of any plaque, obstructive CAD, and plaques with at least two APCs, respectively. *P*-values were smallest for the presence of any plaque, followed by the presence of at least two APCs and obstructive CAD ($P < 0.0001$ for all pairwise comparisons).

Regarding plaque composition, 56.1% (235/419) were associated with noncalcified plaque, 91.9% (385/419) with partially calcified plaque, and 84.7% (355/419) with calcified plaque. All pairwise comparisons were significant ($P < 0.0001$). Manhattan plots of *P*-values are presented in Figure 1A.

Regarding adverse plaque characteristics, low-attenuation, positive remodeling, napkin-ring sign, and spotty calcification were associated with 71.8% (301/419), 79.5% (333/419), 69.0% (289/419), and 89.0% (373/419) of the features, respectively. The *P*-values were the smallest for spotty calcification, followed by positive remodeling, low attenuation, and napkin ring sign. All pairwise comparisons were significant ($P < 0.05$). Manhattan plots of *P*-values are presented in Figure 1B.

Association between plaque characteristics and radiomic features — multivariate analysis

As scanner settings and volumetric properties of the segmented volumes may influence radiomic features, we corrected our results for kVp, mAs, plaque characteristics: noncalcified, low attenuation noncalcified, calcified, and the total volume of the segmentation. After correction, we found a similar proportion of variables to be significant for the presence of any plaque (88.3% [370/419]) and plaques with at least two APCs (76.4% [320/419]), but four parameters (0.9%) showed significant associations with obstructive CAD. Fewer variables were significantly associated with partially calcified (88.5% [371/419]), calcified (80.2% 336/419), and noncalcified plaques (36.5% [153/419]) in univariate analysis.

Regarding APCs, in multivariate analyses, slightly fewer variables were significant for low attenuation: 61.1% (256/419), napkin-ring sign: 61.8% (259/419), and spotty

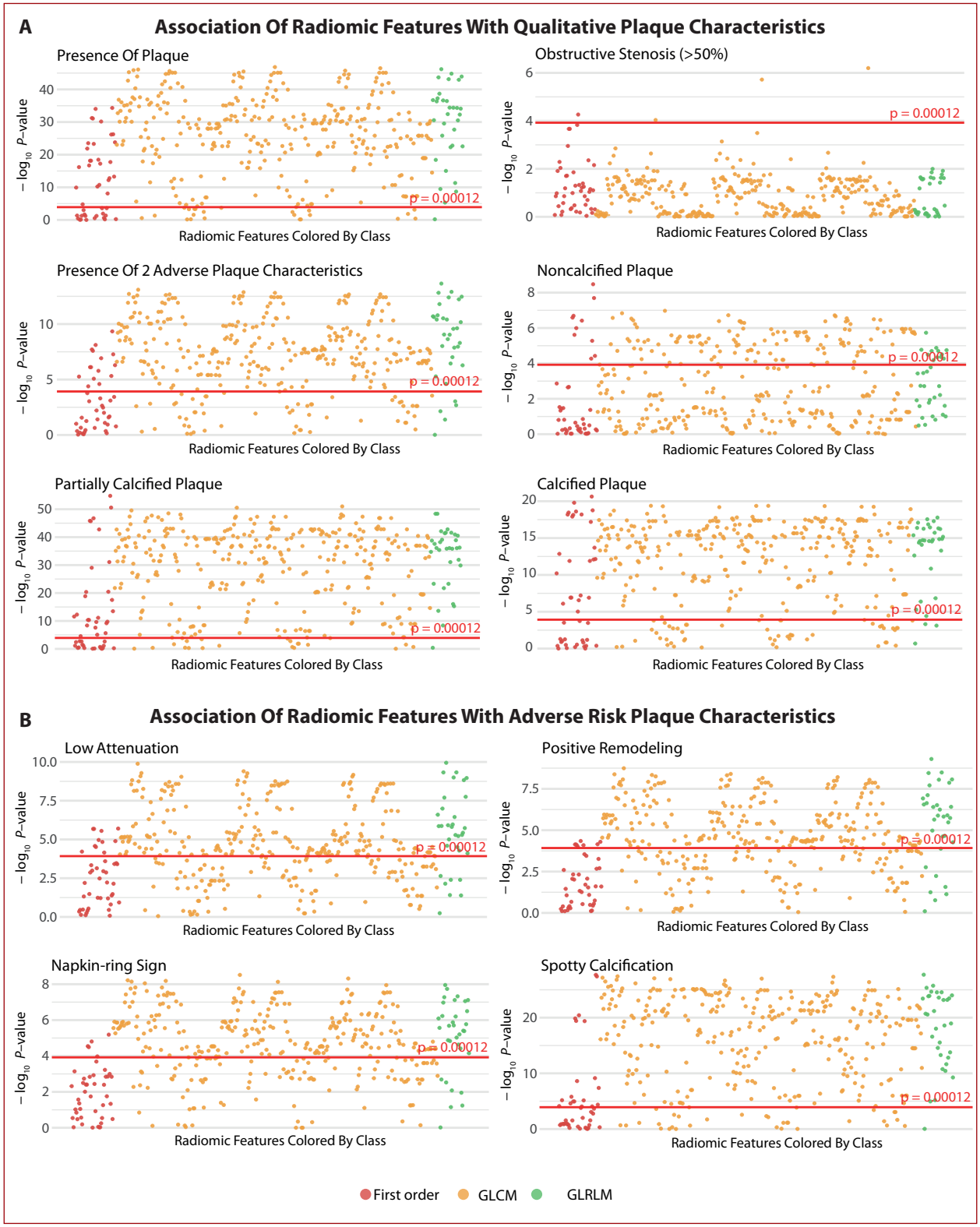

Figure 1. A. Manhattan plot of *P*-values for associations between radiomic features and qualitative plaque characteristics. **B.** Manhattan plot of *P*-values for associations between radiomic features and adverse plaque characteristics

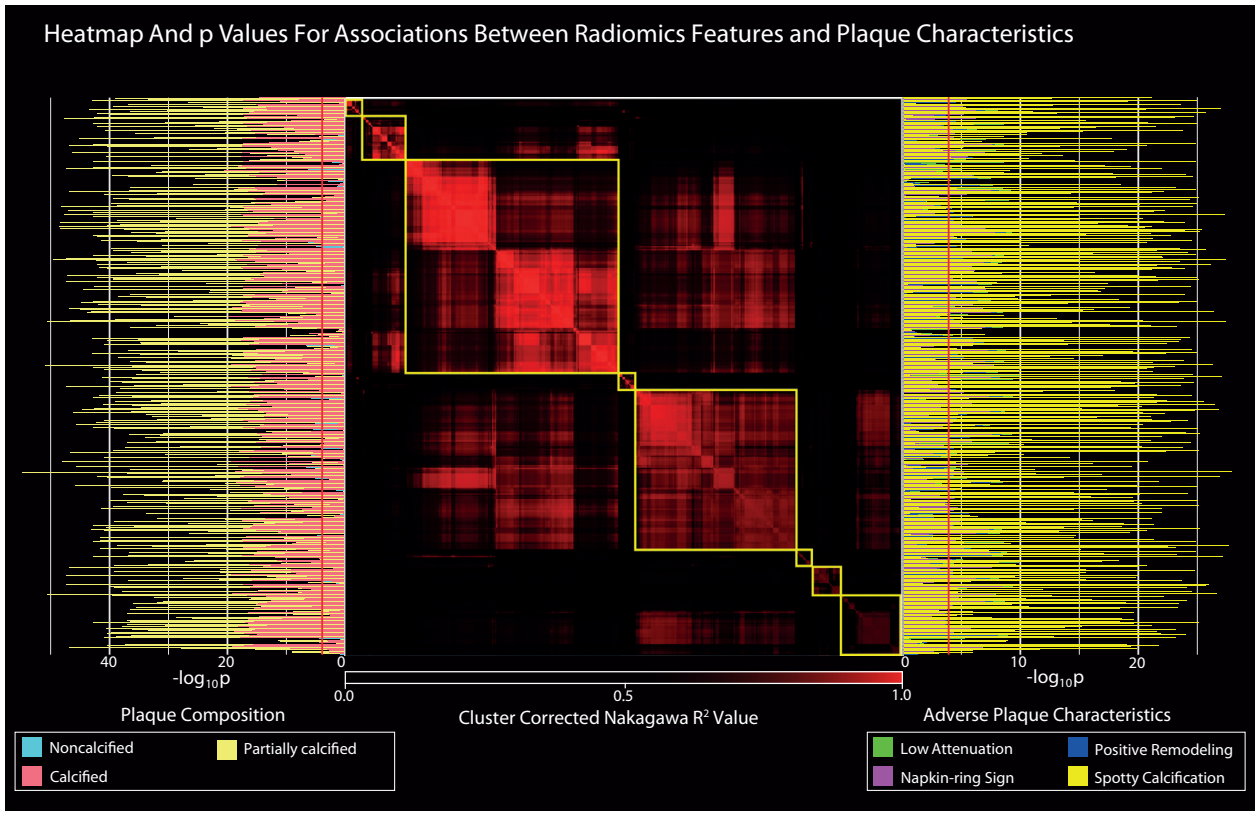

Figure 2. Heatmap of radiomic feature similarities and hierarchical clustering dendrogram with corresponding *P*-values for associations between radiomic features and plaque characteristics

calcification: 84.2% (353/419), and significantly fewer parameters were significant for positive remodeling (61.3% [257/419]). The magnitude of *P*-values showed similar tendencies as univariate analysis.

Association between plaque characteristics and latent morphological features

As individual radiomic features may be representations of the same latent morphology, we conducted hierarchical clustering of our radiomic features based on the similarities between each feature. Using the cluster-corrected Nakagawa's R^2 value as a similarity measure, we created a heatmap representing the similarity network of the radiomic features. We built a hierarchical clustering dendrogram to identify latent morphological features represented by the radiomic signatures. According to the gap statistic, the ideal number of latent features (clusters) was eight. We plotted the *P*-values from each multivariate analysis for each compositional plaque characteristic (i.e. degrees of calcification and individual APCs) at the position of each radiomic feature. We found that none of the clusters were associated specifically with any one of the plaque characteristics. Results are presented in Figure 2.

Magnitude of associations between radiomic features and plaque characteristics

To further elucidate whether the radiomic clusters representing latent morphological features are specifically associated with given plaque types, we plotted the magnitude of the association (effect size: standardized β) in relation to the *P*-values using volcano plots. We found that elements of the 4th and 6th clusters, which contained most of the features, had the largest effect sizes. However, we failed to identify any clear clusters among the associations (Figure 3).

Prediction of plaque characteristics using ML

To validate our findings, we built ML models to predict each plaque outcome using 917 segmentations of 110 individuals. The models were then tested in a separate set of 37 individuals with 292 segmentations. We found that the best radiomics-based ML model outperformed the best conventional method to identify the presence of plaque (area under the curve [AUC], 0.84 vs. 0.77; $P < 0.0001$), obstructive stenosis (AUC, 0.75 vs. 0.74; $P = 0.003$), presence of 2 APCs (AUC, 0.75 vs. 0.70; $P < 0.0001$), presence of noncalcified plaque (AUC: 0.67 vs. 0.57; $P < 0.0001$), and the presence of partially calcified plaque (AUC, 0.87 vs. 0.85; $P = 0.023$). However, the radiomics-based MLE model did not outperform the best conventional method in the case of calcified plaque (AUC, 0.85 vs. 0.87; $P = 0.617$). Results are presented in Figure 4 and Table 2. Regarding APCs, the best radiomics-based ML model outperformed conventional parameters to identify low attenuation plaque (AUC, 0.86 vs. 0.72; $P < 0.0001$) and positively remodeled plaque (AUC, 0.71 vs. 0.66; $P < 0.0001$). However, it failed to outperform conventional metrics to identify napkin-ring

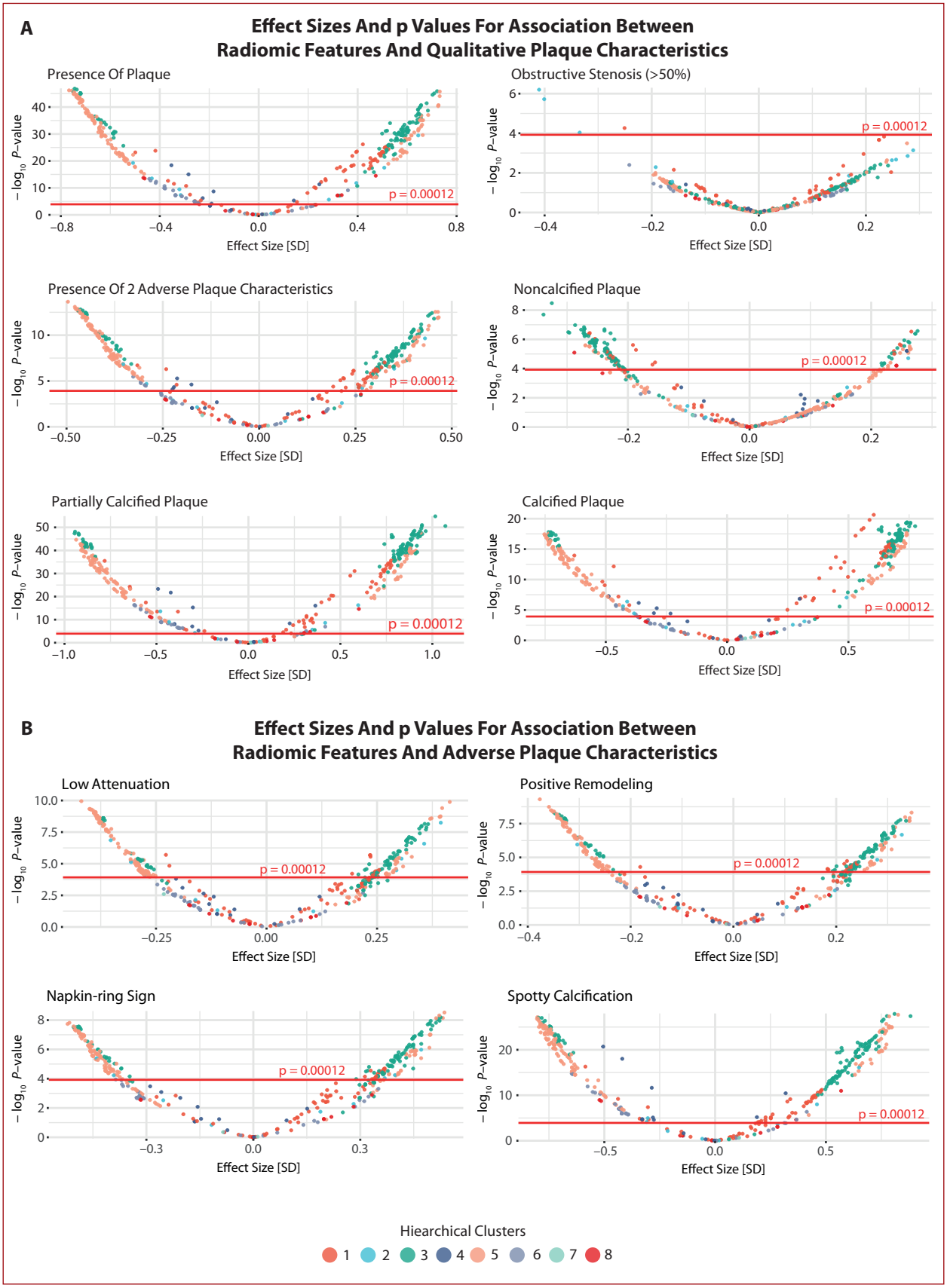

Figure 3. A. Volcano plot of *P*-values and effect sizes for associations between radiomic features and qualitative plaque characteristics. **B.** Volcano plot of *P*-values and effect sizes for associations between radiomic features and adverse plaque characteristics

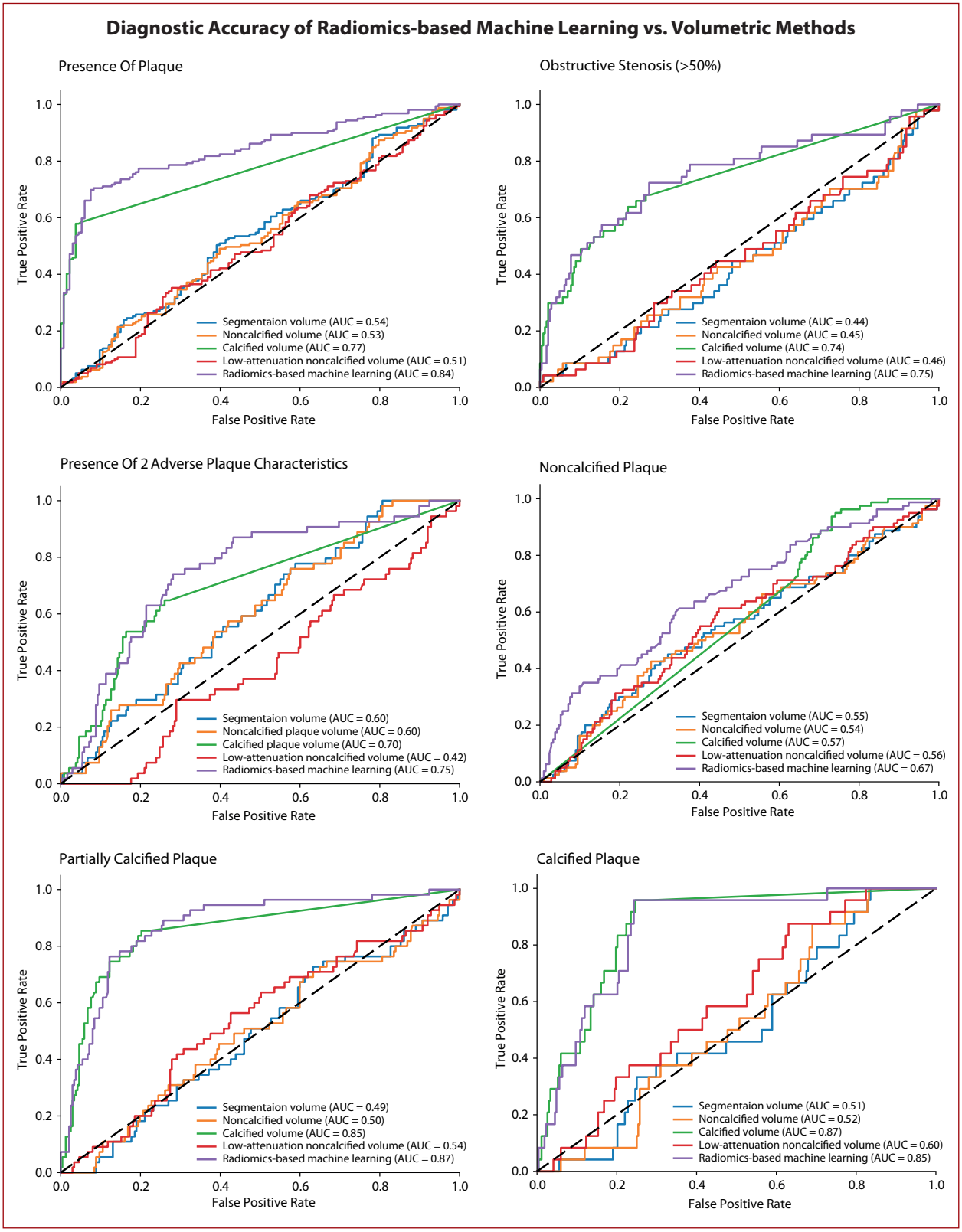

Figure 4. Diagnostic accuracy of radiomics-based machine learning in identifying qualitative plaque characteristics in the patient validation set

Table 2. AUC and *P*-values from ROC analysis to identify qualitative plaque characteristics

	Segmentation volume	Noncalcified volume	Calcified volume	Low attenuation noncalcified volume	Regularized logistic regression	k-nearest neighbors	Random forest	Naïve Bayes	Gaussian process	Decision trees	Neural network
Presence of plaque											
AUC training set	0.51	0.50	0.74	0.55	0.80	0.74	0.78	0.77	0.78	0.50	0.79
AUC test set	0.54	0.53	0.77	0.51	0.84						
P-value compared to ML on test set	<0.0001	<0.0001	<0.0001	<0.0001							
Obstructive stenosis (>50%)											
AUC training set	0.50	0.52	0.69	0.55	0.72	0.61	0.70	0.70	0.71	0.50	0.71
AUC test set	0.44	0.45	0.74	0.46	0.75						
P-value compared to ML on test set	<0.0001	<0.0001	0.003	<0.0001							
Presence of 2 adverse plaque characteristics											
AUC training set	0.52	0.51	0.65	0.52	0.70	0.63	0.69	0.69	0.69	0.50	0.69
AUC test set	0.60	0.60	0.70	0.42	0.75						
P-value compared to ML on test set	<0.0001	<0.0001	<0.0001	<0.0001							
Noncalcified plaque											
AUC training set	0.52	0.53	0.61	0.54	0.66	0.60	0.68	0.66	0.66	0.50	0.66
AUC test set	0.55	0.54	0.57	0.56			0.67				
P-value compared to ML on test set	<0.0001	<0.0001	<0.0001	<0.0001							
Partially calcified plaque											
AUC training set	0.50	0.51	0.84	0.58	0.85	0.81	0.84	0.84	0.83	0.50	0.84
AUC test set	0.49	0.50	0.85	0.54	0.87						
P-value compared to ML on test set	<0.0001	<0.0001	0.023	<0.0001							
Calcified plaque											
AUC training set	0.53	0.55	0.82	0.59	0.83	0.67	0.77	0.80	0.79	0.50	0.74
AUC test set	0.51	0.52	0.87	0.60	0.85						
P-value compared to ML on test set	<0.0001	<0.0001	0.617	<0.0001							

Abbreviations: AUC, area under the curve; ML; machine learning; ROC, receiver operating characteristic

sign (AUC, 0.74 vs. 0.71; $P = 0.325$) and spotty calcification (AUC, 0.81 vs. 0.76; $P = 0.289$). Results are presented in Figure 5 and Table 3.

DISCUSSION

We found that ML-based radiomic analysis of the low-dose, high-resolution, non-contrast CT scan allows for the identification of specific coronary plaque characteristics, including the presence of noncalcified plaque components and APCs. These preliminary findings advance novel research pertaining to high-resolution non-contrast coronary imaging.

The study was based on the assumption that the presence of coronary atherosclerosis and plaque characteristics had a unique pattern on non-contrast CT images that might not be visible to the naked eye but could be identified using radiomics-based ML. Therefore first, we aimed to assess whether the plaques could be identified on the images (segments with plaques vs. without plaques). It was found that the majority of radiomic features differed between coronary segments with and without CAD, even though the segmentations contained not only the vessel wall but also the lumen. Furthermore, significant differences were observed also in high-risk (i.e. two APCs) plaques and all of the individual APC features, even after correcting for imaging and volume characteristics. Weaker associations were found for the presence of significant stenosis and noncalcified plaques probably because plaque characteristics were not necessarily associated with stenosis and noncalcified plaque components showed similar HU values as the lumen without contrast. Current results show that the machine-derived representation of plaque morphology can identify specific plaque characteristics on non-contrast CT images, while the classification scheme developed by humans works only on CCTA images. To validate these results, radiomics-based ML models predicting each plaque characteristics were built, and their predictive power was evaluated on a separate test set. These trained ML models outperformed the classical metrics based on density measures for detection of all but napkin ring sign and calcified plaques. The reason for this might be that in the case of napkin-ring sign, its definition indicates that the low-density core is apparently next to the lumen, but as the lumen cannot be depicted on the non-contrast scans, the algorithm cannot identify this

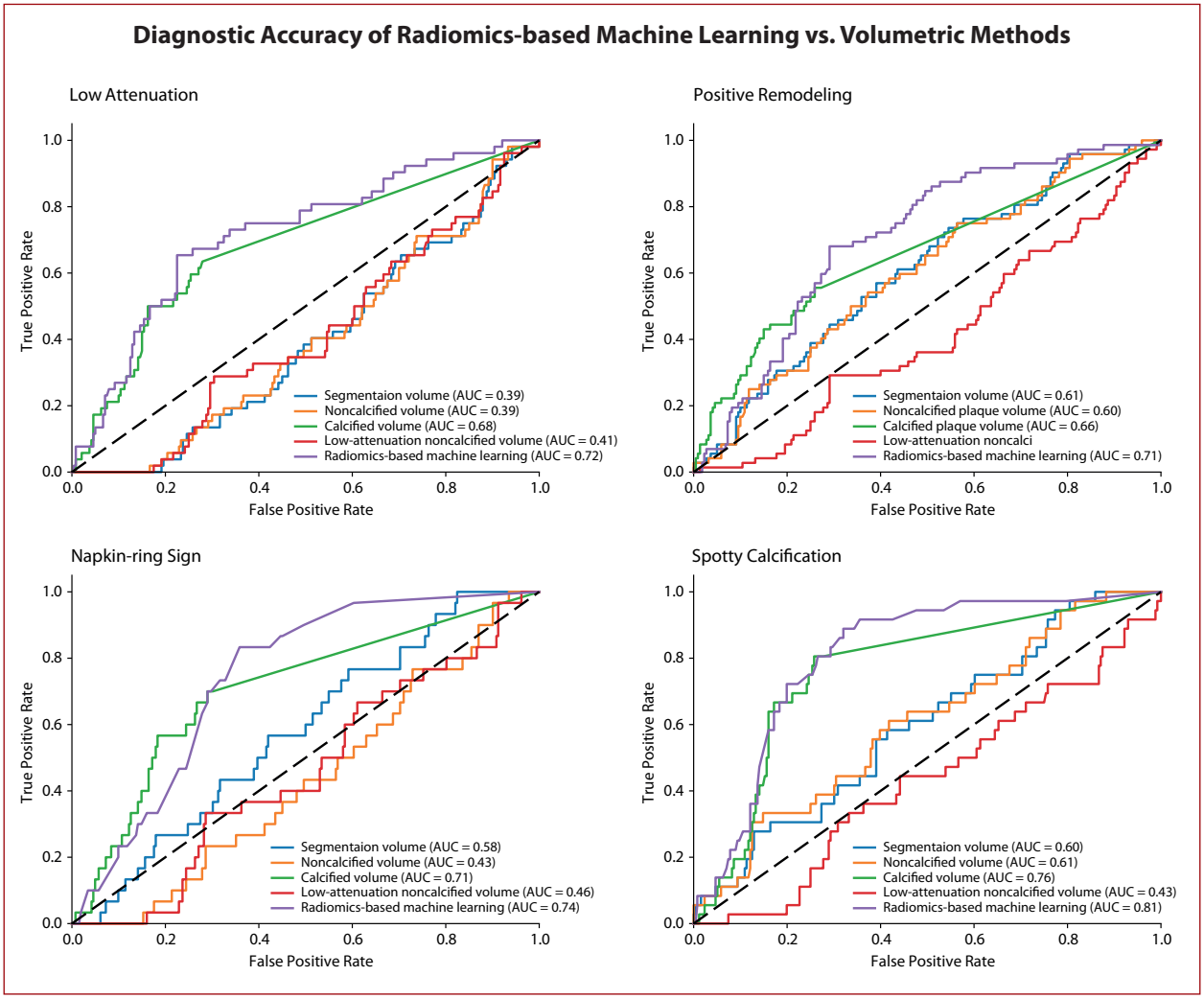

Figure 5. Diagnostic accuracy of radiomics-based machine learning in identifying adverse plaque characteristics in the patient validation set

Table 3. AUC and *P*-values from ROC analysis to identify adverse plaque characteristics

	Segmentation volume	Noncalcified volume	Calcified volume	Low attenuation noncalcified volume	Regularized logistic regression	k-nearest neighbors	Random forest	Naïve Bayes	Gaussian process	Decision trees	Neural network
Low attenuation											
AUC training set	0.49	0.50	0.61	0.53	0.66	0.60	0.64	0.65	0.65	0.50	0.65
AUC test set	0.39	0.39	0.68	0.41	0.72						
P-value compared to ML on test set	<0.0001	<0.0001	<0.0001	<0.0001							
Positive remodeling											
AUC training set	0.55	0.54	0.62	0.50	0.68	0.63	0.69	0.65	0.67	0.50	0.67
AUC test set	0.61	0.60	0.66	0.41			0.71				
P-value compared to ML on test set	<0.0001	<0.0001	<0.0001	<0.0001							
Napkin-ring sign											
AUC training set	0.50	0.51	0.66	0.56	0.69	0.62	0.70	0.65	0.68	0.50	0.69
AUC test set	0.58	0.43	0.71	0.46			0.74				
P-value compared to ML on test set	<0.0001	<0.0001	0.325	<0.0001							
Spotty calcification											
AUC training set	0.52	0.51	0.79	0.55	0.82	0.73	0.82	0.80	0.81	0.50	0.74
AUC test set	0.60	0.61	0.76	0.43			0.81				
P-value compared to ML on test set	<0.0001	<0.0001	0.289	<0.0001							

Abbreviations: see Table 2

specific morphology with high certainty. Also, in the case of calcified plaque, it seems that the simple density metric of calcified volume is equally good. Furthermore, our results also show that for characteristics with limited predictive power of the individual parameters (i.e. significant stenosis), the ML-based combination of these weak predictors resulted in a more accurate model, which is a well-known paradigm in ML research.

While the novel ML radiomic analytic approach is most advanced within tumor diagnostics in oncology, it is being adopted throughout other domains [21–23]. Radiomic analysis improves non-invasive characterization of histological properties of tissue, or its molecular profile, which may translate into clinical benefits including a reduction in invasive diagnostics, streamlining the diagnostic process, better-informed treatment decisions, tracking treatment-related changes, or prediction of clinical outcomes [21–23]. To the best of our knowledge, there are no previous data regarding the radiomic analysis of non-contrast coronary CT images to characterize CAD. Another aspect of this novel analytic approach is utilization of ML methods, suitable for extracting valuable information from various datasets, among others, including ECG, imaging, or clinical data [24, 25]. The few previous analyses of contrast CCTA data indicated improved diagnostic potential of the novel ML-based analysis, compared to the traditional methods, with respect to prediction of functionally significant stenosis, advanced atherosclerotic lesions, cardiovascular event prediction, or lesions with invasive or radionuclide imaging markers of plaque vulnerability [13, 26, 27].

Based on our findings, it may be hypothesized that detection of noncalcified plaque, APC, or stenosis on a non-contrast high-resolution coronary CT scan might be useful for risk evaluation in addition to the coronary calcium score [1–3]. According to recent studies, silent coronary atherosclerosis is present in 9%–16% of the general population with a calcium score of 0 [28, 29]. The presence of low attenuation plaque has been shown to provide cardiovascular risk prediction above that provided by calcium scoring alone [30].

There are several limitations of our study. First of all, the patients were selected on the basis of the presence of at least one single noncalcified plaque with one of the APCs. If we were to analyze consecutive patients undergoing CCTA, the numerical relationships could change.

Another important limitation includes a single center setting, single CT scanner use, and the specific prospective scanning mode application, all of which might impact the image characteristics relevant to radiomics and render the results difficult to replicate with other hardware or protocol settings.

Despite these limitations, this work is a step towards measuring what so far has not been measurable and finding quantitative biomarkers for identifying noncalcified atherosclerotic plaques imaged using non-contrast CT examination.

Radiomic features differ significantly between coronary segments with vs. without specific coronary pathologies on non-contrast high-resolution CT heart images. Using ML, these features improved the detection of coronary pathologies compared to traditional metrics, importantly, with the best performance in the case of noncalcified plaques. Further studies, likely involving larger samples, different scanners, and scanning modes are warranted.

Article information

Conflict of interest: None declared.

Funding: Founded by National Science Center of Poland – grant ID# 2017/27/B/NZ5/02944.

REFERENCES

1. Knuuti J, Wijns W, Saraste A, et al. 2019 ESC Guidelines for the diagnosis and management of chronic coronary syndromes. Eur Heart J. 2020; 41(3): 407–477, doi: 10.1093/eurheartj/ehz425, indexed in Pubmed: 31504439.
2. Achenbach S, Raggi P, Raggi P, et al. Computed tomography for atherosclerosis and coronary artery disease imaging. Discov Med. 2010; 9(45): 98–104, indexed in Pubmed: 20193634.
3. Puchner SB, Liu T, Mayrhofer T, et al. High-risk plaque detected on coronary CT angiography predicts acute coronary syndromes independent of significant stenosis in acute chest pain: results from the ROMICAT-II trial. J Am Coll Cardiol. 2014; 64(7): 684–692, doi: 10.1016/j.jacc.2014.05.039, indexed in Pubmed: 25125300.
4. Xu P, Xue Yi, Schoepf UJ, et al. Radiomics: the next frontier of cardiac computed tomography. Circ Cardiovasc Imaging. 2021; 14(3): e011747, doi: 10.1161/CIRCIMAGING.120.011747, indexed in Pubmed: 33722057.
5. Kolossváry M, Park J, Bang JI, et al. Identification of invasive and radionuclide imaging markers of coronary plaque vulnerability using radiomic analysis of coronary computed tomography angiography. Eur Heart J Cardiovasc Imaging. 2019; 20(11): 1250–1258, doi: 10.1093/ehjci/jez033, indexed in Pubmed: 30838375.
6. Kolossváry M, Jávorszky N, Karády J, et al. Effect of vessel wall segmentation on volumetric and radiomic parameters of coronary plaques with adverse characteristics. J Cardiovasc Comput Tomogr. 2021; 15(2): 137–145, doi: 10.1016/j.jcct.2020.08.001, indexed in Pubmed: 32868246.
7. Lin A, Kolossváry M, Yuvaraj J, et al. Myocardial infarction associates with a distinct pericoronary adipose tissue radiomic phenotype: a prospective case-control study. JACC Cardiovasc Imaging. 2020; 13(11): 2371–2383, doi: 10.1016/j.jcmg.2020.06.033, indexed in Pubmed: 32861654.
8. Newby DE, Adamson PD, Berry C, et al. Coronary CT Angiography and 5-Year Risk of Myocardial Infarction. N Engl J Med. 2018; 379(10): 924–933, doi: 10.1056/NEJMoa1805971, indexed in Pubmed: 30145934.
9. Kolossváry M, Gerstenblith G, Bluemke DA, et al. Contribution of risk factors to the development of coronary atherosclerosis as confirmed via coronary CT angiography: a longitudinal radiomics-based study. Radiology. 2021; 299(1): 97–106, doi: 10.1148/radiol.2021203179, indexed in Pubmed: 33591887.
10. Williams MC, Moss AJ, Dweck M, et al. Coronary artery plaque characteristics associated with adverse outcomes in the SCOT-HEART study. J Am Coll Cardiol. 2019; 73(3): 291–301, doi: 10.1016/j.jacc.2018.10.066, indexed in Pubmed: 30678759.
11. Kolossváry M, Karády J, Szilveszter B, et al. Radiomic features are superior to conventional quantitative computed tomographic metrics to identify coronary plaques with napkin-ring sign. Circ Cardiovasc Imaging. 2017; 10(12): e006843, doi: 10.1161/CIRCIMAGING.117.006843, indexed in Pubmed: 29233836.

12. Kolossvary M. RIA: Radiomics Image Analysis Toolbox for Grayscale Images. 2021.
13. Kolossváry M, Karády J, Kikuchi Y, et al. Radiomics versus visual and histogram-based assessment to identify atheromatous lesions at coronary CT angiography: an ex vivo study. Radiology. 2019; 293(1): 89–96, doi: 10.1148/radiol.2019190407, indexed in Pubmed: 31385755.
14. Pedregosa F, Varoquaux G, Gramfort A, et al. Scikit-learn: machine learning in Python. J Mach Learn Res. 2011; 12: 2825–2830.
15. Van Rossum G, Drake Jr FL. Python reference manual: Centrum voor Wiskunde en Informatica Amsterdam, 1995.
16. Kolossváry M, Szilveszter B, Karády J, et al. Effect of image reconstruction algorithms on volumetric and radiomic parameters of coronary plaques. J Cardiovasc Comput Tomogr. 2019; 13(6): 325–330, doi: 10.1016/j.jcct.2018.11.004, indexed in Pubmed: 30447949.
17. Kolossváry M, Gerstenblith G, Bluemke DA, et al. Contribution of Risk Factors to the Development of Coronary Atherosclerosis as Confirmed via Coronary CT Angiography: A Longitudinal Radiomics-based Study. Radiology. 2021; 299(1): 97–106, doi: 10.1148/radiol.2021203179, indexed in Pubmed: 33591887.
18. Nakagawa S, Johnson PCD, Schielzeth H. The coefficient of determination and intra-class correlation coefficient from generalized linear mixed-effects models revisited and expanded. J R Soc Interface. 2017; 14(134), doi: 10.1098/rsif.2017.0213, indexed in Pubmed: 28904005.
19. Venkatraman E. A distribution-free procedure for comparing receiver operating characteristic curves for a paired experiment. Biometrika. 1996; 83(4): 835–848, doi: 10.1093/biomet/83.4.835.
20. Statistical computing. Computing skills for biologists. 2019: 249–299, doi: 10.2307/j.ctvc77jrc.13.
21. Pinto Dos Santos D, Dietzel M, Baessler B. A decade of radiomics research: are images really data or just patterns in the noise? Eur Radiol. 2021; 31(1): 1–4, doi: 10.1007/s00330-020-07108-w, indexed in Pubmed: 32767103.
22. Li H, El Naqa I, Rong Yi. Current status of Radiomics for cancer management: Challenges versus opportunities for clinical practice. J Appl Clin Med Phys. 2020; 21(7): 7–10, doi: 10.1002/acm2.12982, indexed in Pubmed: 32697032.
23. Gillies RJ, Kinahan PE, Hricak H. Radiomics: images are more than pictures, they are data. Radiology. 2016; 278(2): 563–577, doi: 10.1148/radiol.2015151169, indexed in Pubmed: 26579733.
24. Niedziela JT, Cieśla D, Wojakowski W, et al. Is neural network better than logistic regression in death prediction in patients after ST-segment elevation myocardial infarction? Kardiol Pol. 2021; 79(12): 1353–1361, doi: 10.33963/KP.a2021.0142, indexed in Pubmed: 34704605.
25. Lim DYz, Sng G, Ho WHh, et al. Machine learning versus classical electrocardiographic criteria for echocardiographic left ventricular hypertrophy in a pre-participation cohort. Kardiol Pol. 2021; 79(6): 654–661, doi: 10.33963/KP.15955, indexed in Pubmed: 33885269.
26. Kolossváry M, Park J, Bang JI, et al. Identification of invasive and radionuclide imaging markers of coronary plaque vulnerability using radiomic analysis of coronary computed tomography angiography. J Cardiovasc Comput Tomogr. 2019; 20(11): 1250–1258, doi: 10.1093/ehjci/jez033.
27. Chen Q, Pan T, Wang YiN, et al. A coronary CT angiography radiomics model to identify vulnerable plaque and predict cardiovascular events. Radiology. 2023; 307(2): e221693, doi: 10.1148/radiol.221693, indexed in Pubmed: 36786701.
28. Bergström G, Persson M, Adiels M, et al. Prevalence of subclinical coronary artery atherosclerosis in the general population. Circulation. 2021; 144(12): 916–929, doi: 10.1161/CIRCULATIONAHA.121.055340, indexed in Pubmed: 34543072.
29. Villines TC, Hulten EA, Shaw LJ, et al. Prevalence and severity of coronary artery disease and adverse events among symptomatic patients with coronary artery calcification scores of zero undergoing coronary computed tomography angiography: results from the CONFIRM (Coronary CT Angiography Evaluation for Clinical Outcomes: An International Multicenter) registry. J Am Coll Cardiol. 2011; 58(24): 2533–2540, doi: 10.1016/j.jacc.2011.10.851, indexed in Pubmed: 22079127.
30. Williams MC, Kwiecinski J, Doris M, et al. Low-Attenuation Noncalcified Plaque on Coronary Computed Tomography Angiography Predicts Myocardial Infarction: Results From the Multicenter SCOT-HEART Trial (Scottish Computed Tomography of the HEART). Circulation. 2020; 141(18): 1452–1462, doi: 10.1161/CIRCULATIONAHA.119.044720, indexed in Pubmed: 32174130.